Indian J Phys (September 2020) 94(9):1343–1350
https://doi.org/10.1007/s12648-019-01582-9

ORIGINAL PAPER

Synthesis and characterization of Mn^{+2}-doped zinc silicate as potential green nanophosphor materials

J El Ghoul[1,2]* and N Abdel All[2,3]

[1]Laboratory of Physics of Materials and Nanomaterials Applied at Environment (LaPhyMNE), Faculty of Sciences of Gabes, Gabes University, 6072 Gabes, Tunisia

[2]Department of Physics, College of Sciences, Imam Mohammad Ibn Saud Islamic University (IMSIU), Riyadh 11623, Saudi Arabia

[3]Physics Department, Assiut University, Assiut 71516, Egypt

Received: 14 April 2019 / Accepted: 27 June 2019 / Published online: 14 September 2019

Abstract: Pure and Mn^{+2}-doped Zn_2SiO_4 nanocomposite materials were synthesized using a sol–gel method. The structural, optical, dielectric and magnetic properties of prepared samples were studied using different techniques. X-ray diffraction results show that the dominant phase is willemite (α-Zn_2SiO_4) with rhombohedral structure and average crystallite size varied from 70 to 90 nm. Photoluminescence spectra, PL of Zn_2SiO_4, have two broadband emissions centered at 375 nm and 760 nm. PL spectra of Zn_2SiO_4/Mn is characterized by one dominant peak at 525 and attributed to $^4T_1$–$^6A_1$ transitions of Mn^{2+} ions. Photoluminescence excitation, PLE of Zn_2SiO_4/Mn at 78 K, has strong excitation band from 240 to 300 nm with maximum at about 255 nm (4.9 eV) compared to the bands in UV–Vis range. Dielectric constant, dielectric loss tangent and electrical conductivity of prepared samples are studied as a function of electric field frequency and indicated a strong dependent on Mn^{+2} ions. Zn_2SiO_4 and Zn_2SiO_4/Mn^{+2} have diamagnetic properties at room temperature at 300 K, while Zn_2SiO_4/Mn^{+2} has a ferromagnetic behavior at 5 K.

Keywords: Sol–gel; Nanophosphor materials; Luminescence; Dielectric properties

PACS Nos.: 42.70. − a; 61.43.Gt; 72.80.Tm; 78.55. − m; 61.46. + w; 73.90. + f

1. Introduction

Inorganic phosphors are considered as fundamental materials that have many applications in lighting device displays and information for humankind [1]. In order to improve the structural, morphological and dielectric properties of materials, it can be doped with the appropriate divalent transition metal ions. Generally, the ultrafine particles are controlled by grain boundaries rather than by grains as barriers for electron flow, and then a reduction in the losses of eddy current [2]. The importance of choosing willemite α-Zn_2SiO_4 as a host matrix and doping with a rare earth or transition metal ions is related to its bright luminescence in blue, green and red colors in the electronic systems [3, 4]. Nanophosphor materials have several potential applications such as electronic applications (optoelectronic device, optical fibers and optical fiber amplifiers), electrochemical and catalytic properties, light emitting diodes, industrial applications in aircraft and at a wide frequency range [5, 6]. The conductivity and dielectric properties of nanophosphor materials are strongly dependent on the frequencies and temperatures where their study becomes important to determine the kind of additives that are required to have high quality materials for practical applications [7, 8]. Also it depends on many other factors like preparation, thermal treatment, sintering conditions chemical composition and crystallite structure or size [9]. From many inorganic nanophosphors, α-Zn_2SiO_4/Mn^{2+} is widely used in industry as a green-emitting phosphor for plasma display panels, and this is due to its high luminescence efficiency and its high chemical and physical stabilities [10, 11]. Willemite (Zn_2SiO_4) has phenakite structure belonging to the group of orthosilicates [12] and has many applications such as phosphor host, electrical insulators, glazes and pigments [13, 14]. Also Zn_2SiO_4 has

*Corresponding author, E-mail: ghoultn@yahoo.fr

© 2019 IACS

a rhombohedral structure and characterized by wide energy gap of 5.5 eV, high chemical stability and has advantage of highly saturated color [15]. The chemical synthesis process which it used to prepare the organic–inorganic nanophosphors is called sol–gel method. The process of sol–gel is widely used to have useful product from a solution or precursor suspension materials via hydrolysis and polycondensation. The importance of Sol–gel method is related to the production of a wide variety optical and dielectric materials. This method has advantages in achieving the distribution of dopant ions uniformly in the host matrices [16]. According to our previous work on sol–gel method for synthesis of nanocomposite materials [14, 17, 18], the undoped and Mn-doped Zn_2SiO_4 nanophosphors were synthesized in SiO_2 host matrix by a sol–gel method.

Also the properties of Zn_2SiO_4 and Zn_2SiO_4/Mn nanophosphors, i.e., crystalline properties, luminescence emission and excitation spectra and electrical and magnetic properties were investigated.

2. Experimental details

2.1. Synthesis

Zn_2SiO_4 and Zn_2SiO_4/Mn nanocomposite were synthesized by sol–gel method. The colloid suspension particles in silicate host matrix were performed in three main steps. Firstly, nanocrystalline ZnO and ZnO/Mn aerogels are prepared by sol–gel method under supercritical conditions of ethyl alcohol (EtOH) based on J. EL GHOUL protocol [18]. In the second step, ZnO and ZnO/Mn confined in silica aerogel according to the following process: 0.5 mL of TEOS was dissolved in EtOH and has done constant stirring of the following mixture: TEOS and EtOH, 0.44 mL of water and added 30 mg of nanoparticles powder prepared in the first step. Then, the whole solution is stirred about 30 min until a uniform sol is formed. Then, the sols were transferred to tubes in an ultrasonic bath with adding 100 ml of fluoride acid where a wet gel was formed in a few seconds. Monolithic and white aerogels are formed by supercritical drying in EtOH. Finally, after firing, the aerogel at 1200 °C for 2 h, both Zn_2SiO_4 and Zn_2SiO_4/Mn nanocomposite, was deposited on silica glasses.

2.2. Characterizations

X-ray diffraction (XRD) of Zn_2SiO_4 and Zn_2SiO_4/Mn nanocomposite were measured using a Bruker D5005 powder X-ray diffractometer with CuKα source (1.5418 Å radiation). After the correction of XRD peaks from instrumental broadening, crystallite size of nanocomposites has been calculated by using Scherrer's Eq. (1) [19].

$$G = \frac{0.9\lambda}{B\cos\theta_B} \tag{1}$$

where λ is the X-ray wavelength (λ = 1.5418 Å), θ_B the maximum Bragg diffraction peak (in rad) and B the full width at half maximum (FWHM).

The morphology and particle size of phosphor nanocomposite samples were studied using transmission electron microscopy (TEM, JEM-200CX). For TEM measurements, the specimen was prepared as follows: inserting the as-grown products in EtOH and immersing them in an ultrasonic bath for 15 min. Then, dropping a few drops of the suspension which contain the synthesized nanoparticles into TEM grid. In photoluminescence (PL) measurements, 450-W xenon lamp has been used as an excitation source where the emitted light is collected by an optical fiber and analyzed by a Jobin–Yvon spectrometer HR460 and a multichannel CCD detector (2000 pixels). The photoluminescence excitation (PLE) measurements were performed on a Jobin–Yvon Fluorolog 3–2 spectrometer. The low-temperature measurements were measured by a Janis VPF-600 Dewar with a temperature controller between 78 and 300 K. The magnetic measurements of the nanocomposite samples were performed and characterized by Quantum Design SQUID-VSM magnetometer. Dielectric measurements have been performed in a powder samples. The samples were formed in circular disk-shaped pellets using 2% PVA as a binder and to reduce the brittleness of the pellet by applying 4 ton pressure. The pellets were polished using fine emery paper to make both surfaces smooth and parallel. The opposite surfaces of pellets were exposed to air-drying conducting silver paste to be formed an electrodes. Thereby, the pellets formed parallel plate capacitor geometry to have a good ohmic contact. The electrical impedance and capacitance of the samples were measured in the frequency range from 100 to 1 MHz using a phase-sensitive millimeter (PSM 1700) LCR meter at temperature of 300–573 K. The dielectric constant has been evaluated from: [20]

$$\varepsilon' = \frac{C_s d}{A\varepsilon_0} \tag{2}$$

where C_s is the capacitance, d the pellet thickness, A the cross-sectional area and ε_0 is the permittivity of free space (8.85×10^{-12}(F/m)). Also the complex dielectric constant ε'' of the samples was obtained from the given relation:

$$\varepsilon'' = \varepsilon' \tan\delta \tag{3}$$

where tanδ is the dielectric loss tangent. It is proportional to the energy loss from the applied field, therefore it is denoted as a dielectric loss. The loss tangent (tan δ) has been calculated from:

$$\mathrm{Tan}\delta = \frac{\varepsilon''}{\varepsilon'} \tag{4}$$

A.C. conductivity of the samples was estimated from the relation [21]:

$$\sigma_{ac} = \frac{d}{A}\left(\frac{z'}{z'^2 + z^2}\right) \tag{5}$$

where d is the sample thickness, A effective area; Z is the real part of the complex impedance and Z'' is the imaginary part of that impedance.

3. Results and discussion

3.1. Structural studies

X-ray diffraction patterns of Zn_2SiO_4 (a), Zn_2SiO_4/Mn (b) nanophosphor and Mn-doped ZnO nanopwder (inset) are shown in Fig. 1. The pronounced diffraction peaks in ZnO/Mn are related to the planes of ZnO [4]. XRD patterns of samples are matched well with space group $P6_3mc$ (186) (No. 36-1451) of wurtzite ZnO structure [4, 18]. In addition to ZnO peaks, another secondary phase is observed and related to $ZnOMn_3$ (JCPDS Card 37-1485). The calculated lattice constants were found very close to ZnO ones, i.e., $a = 3.2498$ Å and $c = 5.2066$ Å. These results are in a good agreement with results obtained by J. El Ghoul et al. [22–24]. After the correction of instrumental broadening for all samples, the average crystallite size was estimated as 24 nm.

In this work, a new zincic (α-Zn_2SiO_4) composite was formed where hexagonal ZnO and willemite Zn_2SiO_4 may coexist in this composite [4]. The willemite (α-Zn_2SiO_4) crystals are well-developed, and the analysis shows that the peak identification is indexed to α-Zn_2SiO_4 (JCPDS Card 37-1485) [2–4]. The differences in XRD diffracted peak intensity and its width indicated that the degree of crystallinity of prepared samples is high. The deduced lattice constants $a = 13.944$ Å and $c = 9.314$ Å are very close to those of willemite (α-Zn_2SiO_4) ones [3] and has a rhombohedral structure [2]. XRD diffraction as shown in Fig. 1 indicated that α-phase Zn_2SiO_4 is the most dominant phase, while there are two other phases of silica appeared corresponding to cristobalite and quartz [4]. The average crystallite size of Zn_2SiO_4/Mn has been calculated by Scherrer's equation (Eq. 1) and varied from 70 to 90 nm [2].

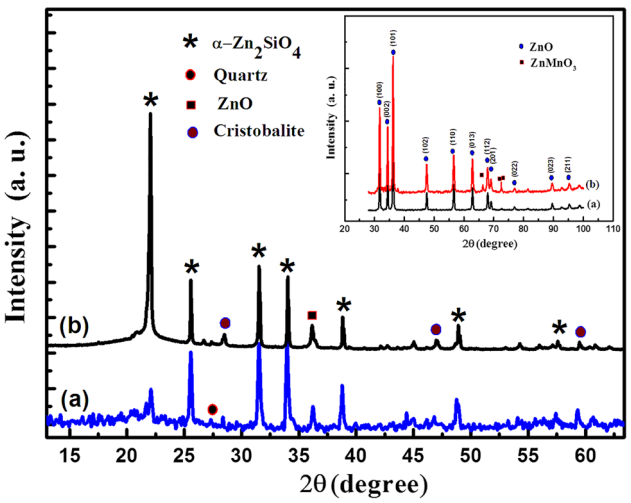

Fig. 1 X-ray diffraction pattern of the (**a**) Zn_2SiO_4 and (**b**) Zn_2SiO_4/Mn. The inset shows the XRD spectra of ZnO/Mn nanopowder

3.2. Morphological studies

The size and morphology of Zn_2SiO_4 and Zn_2SiO_4/Mn nanocomposites have been investigated using transmission electron microscopy, TEM, as shown in Fig. 2. TEM micrographs indicated the well-crystallized Zn_2SiO_4 and Zn_2SiO_4/Mn nanocomposites. At high temperature, 1200 °C, Zn and Si species are moved and diffused inside porous body to form Zn_2SiO_4 phase with particle size greater than 80 nm. Energy dispersive spectroscopy (EDX) analysis has been performed during TEM observations as shown in Fig. 2 and confirmed the XRD results.

3.3. Photoluminescence (PL) and excitation photoluminescence (PLE)

The optical properties of Zn_2SiO_4 and Zn_2SiO_4/Mn nanocomposite were characterized by luminescence properties of nanocomposite in a silica matrix. The PL emission and excitation (PLE) spectra of Zn_2SiO_4 at different temperatures, 78, 160 and 300 K, are shown in Fig. 3. The PL spectra have two broadband emissions; one is centered at 760 nm and another in the range of 375 nm. The interest of the PL spectra is the absence of the usually reported visible emission bands that in the range of 400–650 nm (2.4–2.7 eV). Also the appearance of a strong and wide emission band near infrared (NIR) region and centered around 760 nm that presented beside a near band edge emission which including the bound exciton line. The observed UV–visible emission band of nanophosphor samples were also quite different from what is usually reported in the previous work [4]. However, PLE spectrum as shown in inset of Fig. 3, is detected at 760 nm and has very weak peak at 375 nm (3.3 eV) relative to its value at higher energy. The low energy excitation band is considered due to the carrier excitation in the near band edge of ZnO nanoparticles [4]. Chakrabarti et al. [25] show that the high annealing temperature (1073 K) causes a rapid grain growth and when the radii of the nanoparticles increased up to 8.2 nm, a

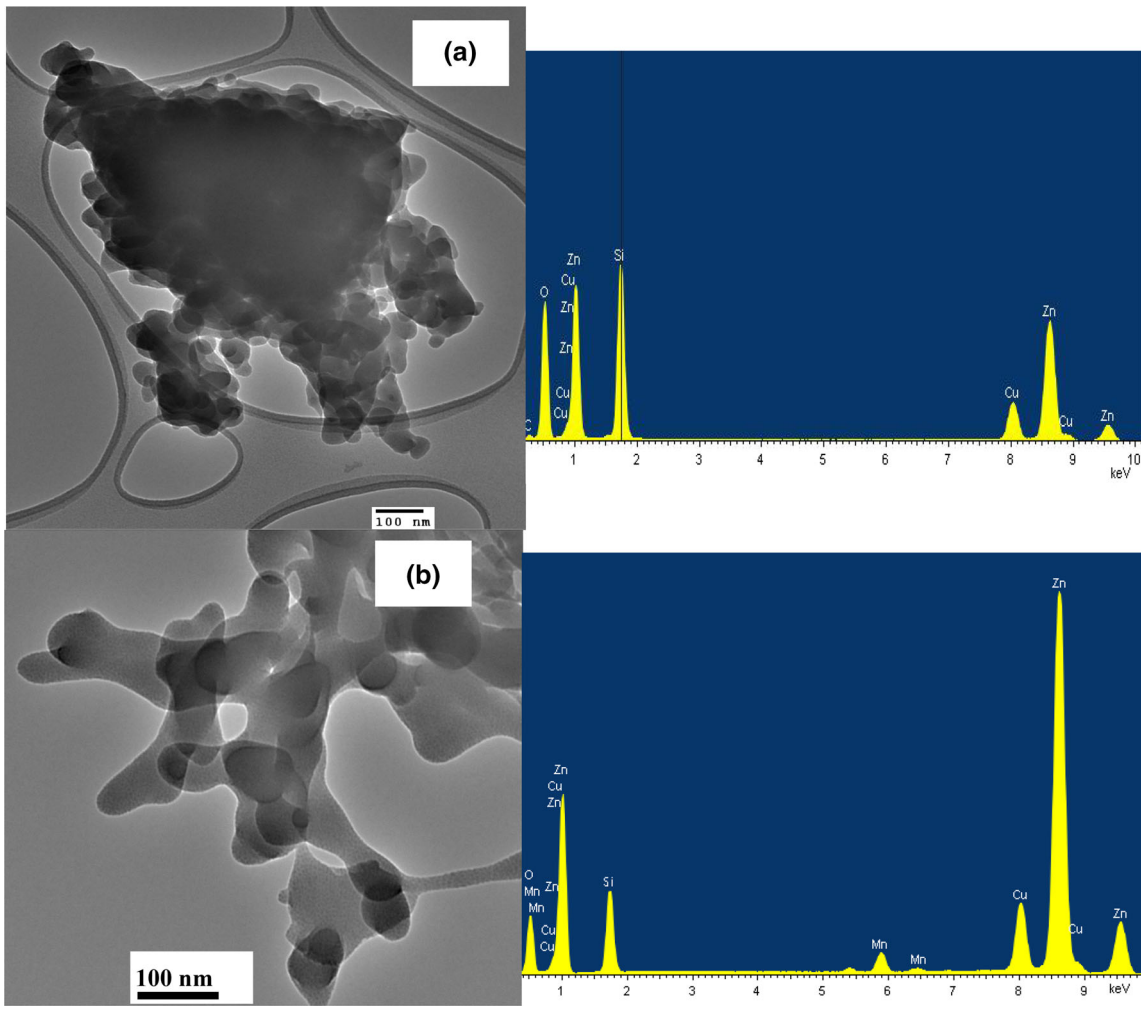

Fig. 2 Typical TEM photograph showing the general morphology (**a**) undoped Zn_2SiO_4 and (**b**) Zn_2SiO_4/Mn and its EDX analysis

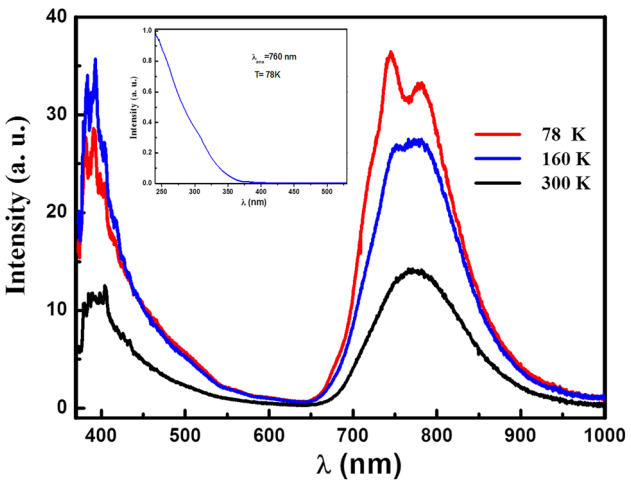

Fig. 3 PL spectrum of a typical Zn_2SiO_4. The inset shows the PLE spectrum of Zn_2SiO_4

band gap of bulk ZnO has obtained. However, excitation processes with photon energies of about 5.4 eV (230 nm) are considered more efficient than the band gap of bulk ZnO. Unfortunately, the higher peak in the PLE spectra could not determine due to the high energy range limit of the used setup. The luminescence emission band at 760 nm is produced from the absorption of Zn_2SiO_4 nanocomposite and may be attributed to the contribution at the formation of NBOHs excited at the spectral region of $h\nu \geq 5.4$ eV. The PL spectra of Zn_2SiO_4/Mn nanocomposite were measured at various temperature, 78, 160 and 300 K, as shown in Fig. 4. The PL spectra have strong luminescence band centered at 525 nm. The green emission band is related to an electronic transition of $^4T_1(^4G) \rightarrow {}^6A_1(^6S)$ that peaking at the wavelength of 525 nm and a parity forbidden emission of Mn^{2+} ions [15]. The relative intensity of PL spectra of Zn_2SiO_4/Mn nanocomposite is decreased with an increase in temperature, while the temperature did not affect the position of emission band spectra as shown in Fig. 4. It is generally known, the luminescence of the Mn^{2+} ions depend on the field of Zn_2SiO_4 host crystal. If Mn^{2+}

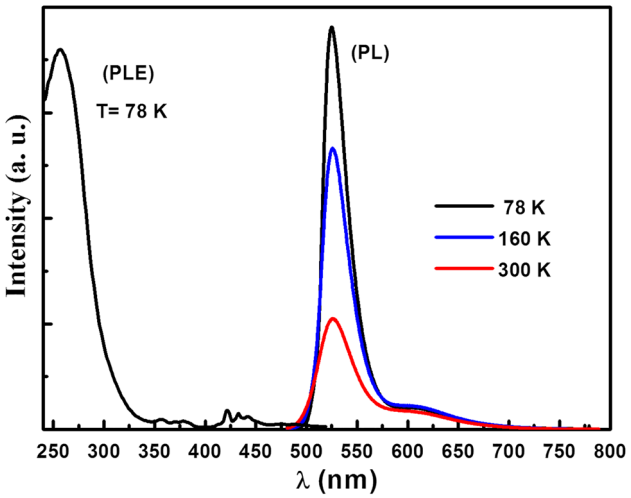

Fig. 4 PL and PLE spectra of a typical Zn_2SiO_4/Mn

ions were hosted in a higher crystallinity of Zn_2SiO_4, it will receive a stronger crystal field.

Furthermore, the PLE spectra of Zn_2SiO_4/Mn at low temperature, 78 K, show a strong excitation band from 240 to 300 nm with a maximum at about 255 nm (4.9 eV) compared to the bands in UV–Vis range. The emission band at 255 nm is considered responsible for the emission at 525 nm and is fully agreed with the excitation spectrum that was previously measured for Zn_2SiO_4/Mn [26]. The broad excitation peak at 255 nm could be attributed to a transition of charge transfer (Mn^{2+}) from the divalent ground state to conduction band (CB), while the green emission band at 525 nm is due to radiative transition from the $^4T_1$ (^4G) excited state to $^6A_1$ (^6S) ground state as shown in Fig. 4.

There are other bands of Mn^{2+} (d–d) transitions that were observed at wavelengths between 350 and 500 nm. These bands with low intensities can be due to the crystal field splitting of the 4D and 4G levels as illustrated in the Orgel diagram for Mn^{2+} [27, 28].

3.4. Dielectric properties

3.4.1. Dielectric constant

The relation between dielectric constant (ε') versus frequency (100–1 MHz) of Zn_2SiO_4 and Zn2SiO4/Mn nanophosphors at different temperatures is shown in Fig. 5. The dielectric constant at different temperatures is decreased with an increase in frequency where it decrease rapidly at lower frequency and became slow at higher frequency. So that ε' decreases exponentially with increasing frequency and become almost frequency independent at high frequency [8]. Zn_2SiO_4 and Zn2SiO4/Mn nanocomposites show a normal dielectric (ε') behavior where it decreases with an increase in frequency. In Fig. 5(a), Zn_2SiO_4 has a dielectric constant, ε' that decreases with an increase in frequency and increase in temperature from 303 to 573 K. However, ε' of Zn_2SiO_4/Mn^{2+} is decreased with an increase in frequency but increased with an increase in temperature up to 523 K, and then decreased at 573 K as shown in Fig. 5(b). The increase in ε' with temperature can be due to the weakling of binding force between molecules/atoms with increasing temperature. Molecules/atoms have more vibrations with increasing temperature which in turn increase the polarization, and hence increase the dielectric constant [29]. In general, there are four main contributions to the polarization in nanophosphors materials, namely electronic, atomic, dipolar and interfacial polarization. The electronic and atomic polarizations are temperature independent and considered as an important types at high frequencies, while dipolar and interfacial polarization are a temperature dependent, and they are playing a dominant role at lower frequencies. The interfacial polarization is increased with temperature, while dipolar polarization decreases with temperature [30].

Therefore, the increase in dielectric constant at lower frequency of Zn_2SiO_4/Mn^{2+} is attributed to the interfacial polarization which it becomes the main contributor to the dielectric constant. However, the decrease in dielectric constant at lower frequency of Zn_2SiO_4 may be due to the dominance of a dipolar polarization. The polarization types that lowered the values of dielectric constant which it can be considered for the high-frequency applications to reducing the eddy current effect.

3.4.2. Dielectric loss (tan.)

The variation of dielectric loss tangent (tan δ) versus frequency at different temperatures of Zn_2SiO_4 and Zn_2SiO_4/Mn^{+2} nanocomposites is shown in Fig. 6. The dielectric loss is decreased with an increase in frequency of the applied ac electric field. This decrease is attributed to a certain frequency where the charge carriers cannot follow the frequency of applied field. In Fig. 6(a), dielectric loss decreased rapidly at low frequency and has slower decrease in high frequency; then, it becomes almost frequency independent. The behavior at low frequency can be explained corresponding to high resistivity due to grain boundary. More energy is required to exchange through the interaction of cation valence state, so that the loss becomes high. The dielectric loss in Fig. 6(b) is increased with an increase in temperature that is due to enhanced hopping of thermally energetic electrons. Moreover, this is consistent with the mathematical definition of loss tangent (tan δ) which is equal to ($\varepsilon''/\varepsilon'$) (Eq. 4), where ε'' and ε' *are* represented as a measure of current resistivity and capacitive

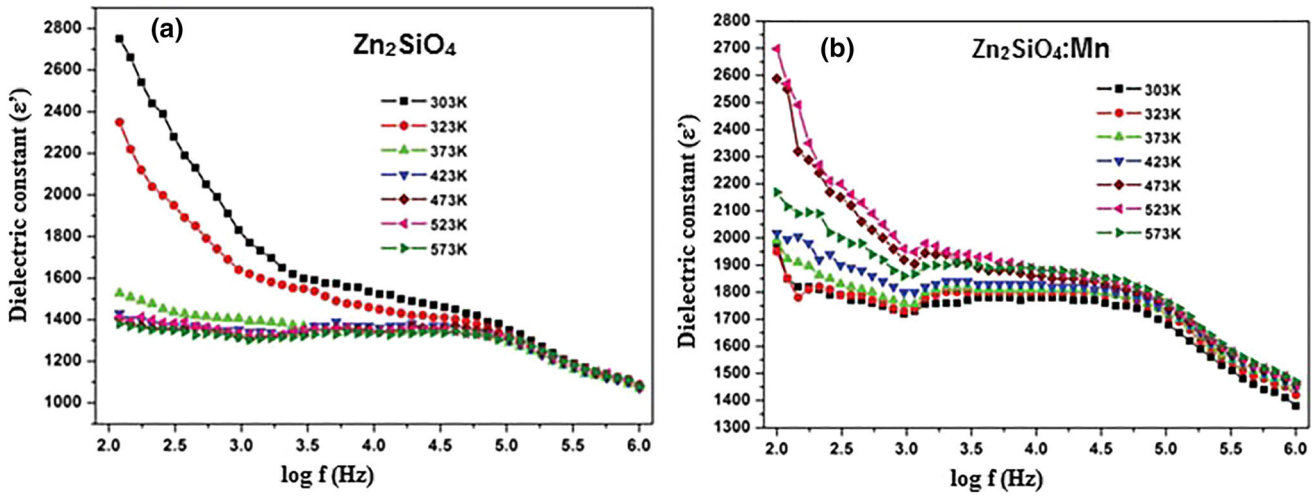

Fig. 5 Dielectric constants at different temperatures for the pure and Zn_2SiO_4/Mn nanophosphors powders

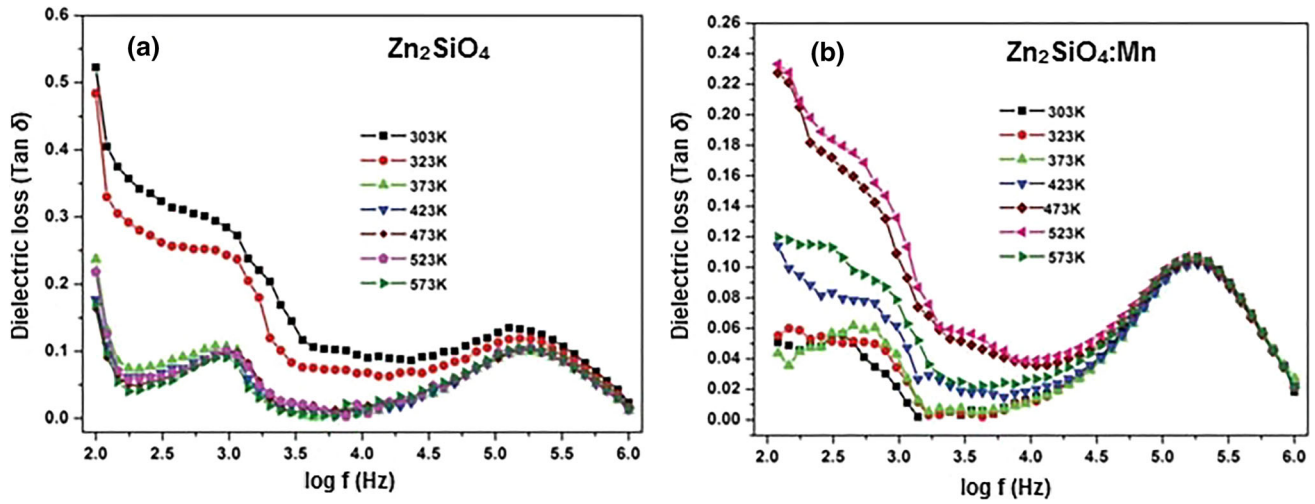

Fig. 6 Dielectric loss with frequency at different temperatures for the pure and Zn_2SiO_4/Mn nanophosphors powders

current in the electrical equivalent circuit of the sample, respectively.

3.4.3. Electrical conductivity

The relation between electrical conductivity versus frequency of Zn_2SiO_4 and Zn2SiO4/Mn^{+2} nanophosphors at different temperatures, 303–573 K, is shown in Fig. 7. Electrical conductivity increased slowly at low frequency, while it highly increases with an increase in frequency. In low-frequency regions, the electrical conductivity is almost constant, and the transport takes place on infinite paths. While in regions with strong increasing conductivity, the transport is dominated by contributions from hopping infinite clusters. Therefore, the interesting region is taken when the high-frequency cutoff started to play a role. The σ_{ac} conductivity of the samples has been calculated using the relation in Eq. (5). At low frequency, it remains almost constant, while increases abruptly in the high-frequency region. The increase in σ_{ac} conductivity with frequency is considered as hopping model in distinguishing the different characteristic regions of frequency [31]. It is well-known that the electrical conduction mechanism is the same as that of dielectric polarization. The electrical conduction mechanism has been explained according to the electron hopping model [30–32]. The hopping frequency of the applied field will increase according to the increase in the applied electric field frequency. Also, the hopping frequency of the electrons between cation ions states at adjacent octahedral site is increased due to the thermally activated electrons that lead to increase in the conductivity.

The σ_{ac} conductivity of Zn_2SiO_4/Mn^{+2} is increased with an increase in temperature as shown in the inset of Fig. 7(b). This increase can be related to the release of

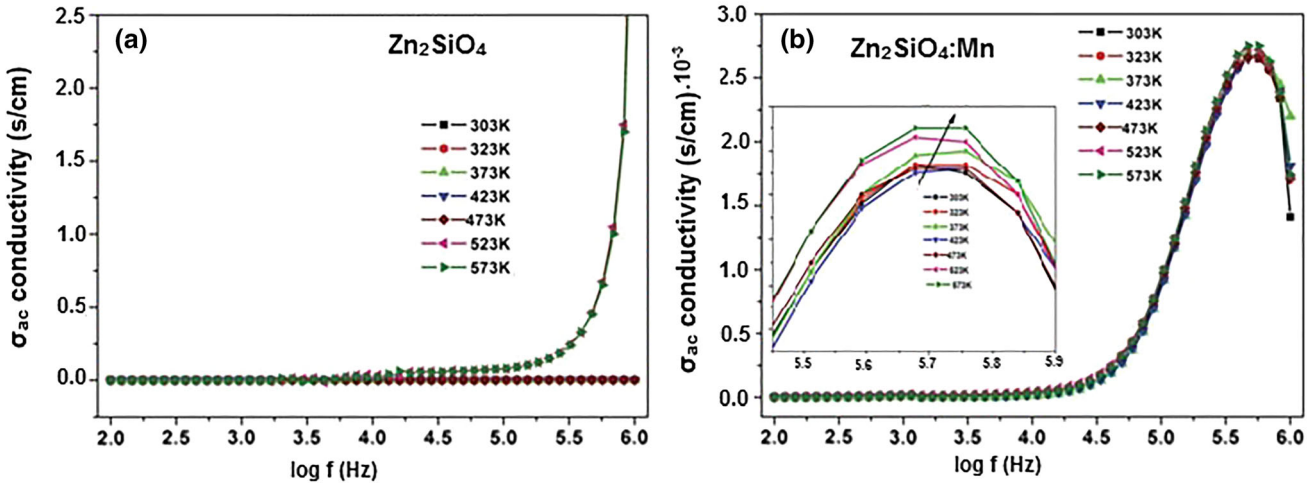

Fig. 7 Electrical conductivity (σ_{ac}) with frequency at different temperatures for the pure and Zn_2SiO_4/Mn nanophosphors powders

space charge at the electrode–sample interface. Therefore, the increase in frequency enhanced the hopping frequency of charge carriers and caused increase in the conductivity.

3.5. Magnetic properties

Magnetization field (M–H) hysteresis loop curves for Zn_2SiO_4 and Zn_2SiO_4/Mn^{+2} nanophosphors are shown in Fig. 8. The M–H curves at 300 K indicated a completely diamagnetic behavior for all samples with a negative magnetic susceptibility. The measured M–H curve of Zn_2SiO_4/Mn^{+2} at 5 K is shown a clear ferromagnetic behavior [33]. Then, the deduced values of saturation magnetization (M_s) and coercive field (H_c) for Zn_2SiO_4/Mn^{+2} are 0.0027 emu/g and 98.6 Oe, respectively. Moreover, Zn_2SiO_4 and Zn_2SiO_4/Mn^{+2} nanophosphors have diamagnetic properties at room temperature. Therefore, the obtained results suggested that these types of multifunctional, multicolor emitting nanophosphors are considered as a promising application in the fields of full color displays, biomedical science and others [34].

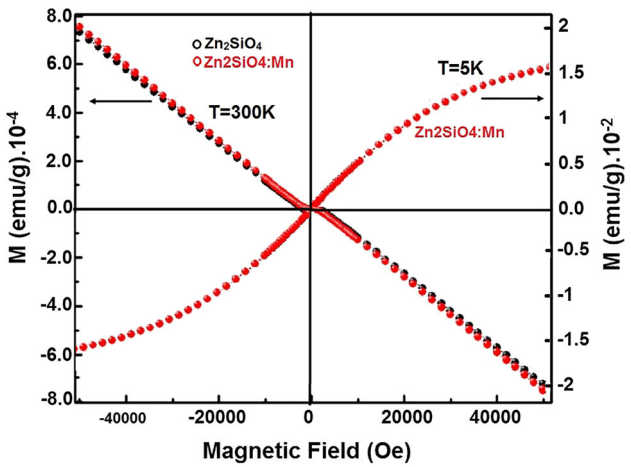

Fig. 8 M–H curves for Zn_2SiO_4 and Zn_2SiO_4/Mn nanophosphors at 300 K and 5 K

4. Conclusion

Zn_2SiO_4 and Mn-doped Zn_2SiO_4 nanophosphor materials were synthesized using sol–gel method. XRD results indicated that the willemite (α-Zn_2SiO_4) is the most dominant phase with rhombohedral structure, and average crystallite size was varied from 70 to 90 nm. TEM micrographs indicated the well-crystallized Zn_2SiO_4 and Zn_2SiO_4/Mn nanocomposite. The crystalline phase of Zn2SiO4/Mn has been investigated by TEM images and XRD analysis. The PL emission and excitation (PLE) spectra of Zn_2SiO_4 were shown strong and wide emission band near infrared (NIR) region and centered around 760 nm. This emission is due to the absorption of Zn_2SiO_4 nanocomposite which may be attributed to the contribution at the formation of NBOHs excited at the spectral region of $h\nu \geq 5.4$ eV. The PLE spectra at low temperature, 78 K, of Zn_2SiO_4/Mn show a strong excitation band from 240 to 300 nm with a maximum at about 255 nm and are considered responsible for the emission at 525 nm. The green emission band at 525 nm is due to a radiative transition from the $^4T_1$ (^4G) excited state to $^6A_1$ (^6S) ground state. The dielectric constant ε and loss tangent (tan δ) of Zn_2SiO_4 and Zn2SiO4/Mn are decreased with an increase in frequency of applied electric field. The ac conductivity (σ_{ac}) of samples was slowly increased at low frequency and highly increased at high frequency. The σ_{ac} of Zn_2SiO_4/Mn^{+2} show an increase in the conductivity with an increase in temperature. The Zn_2SiO_4 and Zn_2SiO_4/Mn^{+2} nanophosphors exhibited diamagnetic properties at

room temperature, 300 K, while at lower temperature (5 K), Zn_2SiO_4/Mn shows a ferromagnetic behavior. According to structural, optical, dielectric and magnetic properties of the synthesized samples, they became an important candidate as a potential material of significant applications. These promising results indicated the importance of using transition metals of luminescence nanophosphors for developing plasma display panels (PDPs), full color displays, biomedical science and other important applications.

References

[1] C Feldmann, T Jüstel, C R Ronda and P J Schmidt *Adv. Funct. Mater.* **13** 511 (2003)
[2] A Verma, T C Goel, R G Mendiratta and M I Alam *Mater Sci. Eng. B* **60** 156 (1999)
[3] S R Lukic, D M Petrovic, L J Dacanin and M Marnovic *Opto Electron Adv. Mater.* **10** 2748 (2008)
[4] M K Radenka, A Zelijka, M Mitric, D D Mirosalv and G Brik Mikhail *Appl. Phys. A* **104** 483 (2011)
[5] T Li, H Qiu and W Ping *Thin Solid Films* **515** 3905 (2007)
[6] B Wu, J Qiu, M Peng, J Ren, X Jiang and C Zhu *Mater. Res. Bull.* **42** 762 (2007)
[7] M A Elkestawy *Alloys Compd.* **492** 616 (2010)
[8] S A Saafan and S T Assar *Magn. Magn. Mater.* **324** 2989 (2012)
[9] S Mazen, S F Mansour, E Dhahri, H M Zaki and T A Elmosalami *Alloys Compod.* **470** 294 (2009)
[10] Y Jiang, J Chen, Z Xie and L Zheng *Mater. Chem. Phys.* **120** 313 (2010)
[11] M Takesue, H Hayashi and R L Smith *Prog. Cryst. Growth Charact. Mater.* **55** 98 (2009)
[12] L El Mir, A Amlouk and C Barthou *Phys. Chem. Solids* **67** 2395 (2006)
[13] Q Y Zhang, K Pita, W Ye and W X Que *Chem. Phys. Lett.* **351** 163 (2002)
[14] J El Ghoul, K Omri, L El Mir, C Barthou and S Alaya *J. Luminesc.* **132** 2288 (2012)
[15] R Selomulya, S Ski, K Pita, C H Kam, Q Y Zhang and S Buddhu *Mater. Sci. Eng. B* **100** 136 (2003)
[16] S Sakka, H Kozuka *Hand Book of Sol–Gel Science and Technology Processing Characterization and Applications. 1. Sol–Gel Processing* (New York: Kluwer Academic Publishers) (1999)
[17] J El Ghoul, I Ghiloufi, L El Mir *J. Luminesc.* **170** 180 (2016)
[18] J El Ghoul *Mater. Sci. Mater. Electron.* **29** 2999 (2018)
[19] B D Cullity *Elements of X-ray Diffractions Addison-Wesley Reading* (MA) Vol. 102 (1978)
[20] K M Batoo *Phys. Chem. Solids* **72** 1400 (2011)
[21] B C Babu, V Naresh, B J Prakash and S Buddhudu *Ferroelectr. Lett. Sect.* **38** 114 (2011)
[22] J El Ghoul, C Barthou and L El Mir *Phys. E Low Dimens. Syst. Nanostruct.* **44** 1910 (2012)
[23] J El Ghoul, C Barthou and L El Mir *Superlattices Microstruct.* **51** 942 (2012)
[24] J El Ghoul, C Barthou, M Saadoun and L El Mir *Phys. B* **405** 597 (2010)
[25] S Chakrabarti, D Das, D Ganguli and S Chaudhuri *Thin Solid Films* **441** 228 (2003)
[26] A Patra, G A Baker and S N Baker *J. Luminesc.* **111** 105 (2005)
[27] C Barthou, J Benoit, P Benalloul and A Morell *J. Electrochem. Soc.* **141** 524 (1994)
[28] L E Orgel *Chem. Phys.* **23** 1819 (1955)
[29] M Goswami, S K Deshpande, R Kumar and G P Kothiyal *Phys. Chem. Solids* **71** 739 (2010)
[30] A Thakur, P Mathur and M Singh *Phys. Chem. Solids* **68** 378 (2007)
[31] K M Batoo, S Kumar, C G Lee and A muddin *Curr. Appl. Phys.* **9** 1072 (2009)
[32] I Soibam, S Phanjoubam, H B Sharma, K N K Sarma, R Laishram and C Prakash *Solid State Commun.* **148** 399 (2008)
[33] O M Lemine, K Omri, B Zhang, L El Mir, M Sajieddine, A Alyamani and M Bououdina *Superlattices Microstruct.* **52** 793 (2012)
[34] Q Su, H Y Wang, S Z Xu, *Chin. Rare Earth Soc.* **3** 33 (1985)

Publisher's Note Springer Nature remains neutral with regard to jurisdictional claims in published maps and institutional affiliations.